Cerebral Cortex February 2014;24:315–327
doi:10.1093/cercor/bhs310
Advance Access publication October 18, 2012

Fetal Brain mTOR Signaling Activation in Tuberous Sclerosis Complex

Victoria Tsai[1], Whitney E. Parker[1], Ksenia A. Orlova[1], Marianna Baybis[1], Anthony W.S. Chi[1], Benjamin D. Berg[1], Jacqueline F. Birnbaum[1], Jacqueline Estevez[1], Kei Okochi[1], Harvey B. Sarnat[2], Laura Flores-Sarnat[2], Eleonora Aronica[3] and Peter B. Crino[1]

[1]PENN Epilepsy Center, Department of Neurology and University of Pennsylvania Medical Center, Philadelphia, PA 19104, USA, [2]University of Calgary and Alberta Children's Hospital, Calgary, Alberta, Canada T3B 6A8 and [3]Department of (Neuro)Pathology, Academic Medical Center, University of Amsterdam, 1105AZ Amsterdam, and Stichting Epilepsie Instellingen Nederland, Heemstede, The Netherlands

Address correspondence to: Dr Peter B. Crino, Department of Neurology, University of Pennsylvania, 3 West Gates Building, 3400 Spruce Street, Philadelphia, PA 19104, USA. Email: peter.crino@uphs.upenn.edu

Tuberous sclerosis complex (TSC) is characterized by developmental malformations of the cerebral cortex known as tubers, comprised of cells that exhibit enhanced mammalian target of rapamycin (mTOR) signaling. To date, there are no reports of mTORC1 and mTORC2 activation in fetal tubers or in neural progenitor cells lacking Tsc2. We demonstrate mTORC1 activation by immunohistochemical detection of substrates phospho-p70S6K1 (T389) and phospho-S6 (S235/236), and mTORC2 activation by substrates phospho-PKCα (S657), phospho-Akt (Ser473), and phospho-SGK1 (S422) in fetal tubers. Then, we show that Tsc2 shRNA knockdown (KD) in mouse neural progenitor cells (mNPCs) in vitro results in enhanced mTORC1 (phospho-S6, phospho-4E-BP1) and mTORC2 (phospho-Akt and phospho-NDRG1) signaling, as well as a doubling of cell size that is rescued by rapamycin, an mTORC1 inhibitor. Tsc2 KD in vivo in the fetal mouse brain by in utero electroporation causes disorganized cortical lamination and increased cell volume that is prevented with rapamycin. We demonstrate for the first time that mTORC1 and mTORC2 signaling is activated in fetal tubers and in mNPCs following Tsc2 KD. These results suggest that inhibition of mTOR pathway signaling during embryogenesis could prevent abnormal brain development in TSC.

Keywords: epilepsy, fetal tuber, rapamycin, TSC2, tuberous sclerosis complex

Introduction

Tuberous sclerosis complex (TSC) is an autosomal dominant disorder resulting from mutations in either *TSC1* or *TSC2* genes, characterized neurologically by intractable epilepsy, cognitive disability, and autism spectrum disorders. Cortical tubers are malformations of the cerebral cortex, which are detected as early as 20 weeks gestation (Park et al. 1997) and identified in over 80% of TSC brain specimens (Sparagana and Roach 2000; DiMario 2004; Crino et al. 2006). Tubers exhibit severely disorganized lamination and contain cells with abnormal cellular morphology, specifically enhanced cell size (cytomegaly). While tubers are linked closely to epileptogenesis in TSC, there is a debate as to whether there is a relationship between tuber number or "tuber burden" and severity of neurocognitive deficits in TSC patients (Jambaque et al. 1991; Marcotte and Crino 2006; Zaroff et al. 2006; Ess and Roach 2012; Tillema et al. 2012).

The encoded TSC1 and TSC2 proteins form a functional heterodimeric complex that inhibits the mammalian target of rapamycin (mTOR) signaling pathway (Wullschleger et al. 2006; Huang and Manning 2008). Loss of function mutations in *TSC1* or *TSC2* in neuroglial progenitor cells lead to constitutive activation of the mTOR cascade as evidenced by phosphorylation of p70 S6 kinase 1 (P-p70S6K1; T389) and ribosomal protein S6 (P-S6; S235/236) in pediatric and adult human tuber specimens and TSC animal models (Huang and Manning 2008). Extant transgenic mouse strains lacking either *Tsc1* or *Tsc2* under conditional cell-specific promoters (e.g., hGFAP and Synapsin1) exhibit variable morphological and functional changes including astrocytosis, laminar disorganization, cytomegaly, spontaneous seizures, and decreased survival (Uhlmann et al. 2002; Wang et al. 2007). Conditional *Tsc2* deletion in mouse radial glial cells ($Tsc2^{bGFAP}Cre$) produces megalencephaly and cortical lamination defects (Way et al. 2009). $Tsc2^{bGFAP}Cre$ knockout mice have been shown to have a more severe seizure phenotype than $Tsc1^{bGFAP}Cre$ knockout mice (Zeng et al. 2011). In most *Tsc1* or *Tsc2* mouse mutants, transgene expression occurs across much of the developing telencephalon as opposed to within focal brain regions similar to tubers in TSC. Recently, a murine model was reported in which biallelic *Tsc1* mutations engineered in neuroglial progenitor cells caused focal brain malformations (Feliciano et al. 2011). Generating focal malformations on a background of morphologically intact cortex provides an attractive strategy to test the new pharmacotherapies on lesion formation, as well as the surrounding cortex.

Since hyperactivation of mTOR signaling has thus far been demonstrated in tubers only at postnatal time points and since to date, no studies have evaluated mTOR complex 2 (mTORC2) signaling in TSC brain, we examined the phosphorylation status of mTORC1 substrates P-p70S6K1, P-S6, and c-myc and mTORC2 complex substrates P-PKCα (S657), P-Akt (Ser473), P-SGK1 (S422), and P-NDRG1 (Thr346) in human fetal tubers to determine the activation state of mTORC1 and mTORC2 during fetal development. Because recent human and animal genotype-phenotype analyses have demonstrated that *TSC2* gene mutations are associated with a more severe clinical phenotype than *TSC1*, and because many of the existing conditional knockout mouse strains target *Tsc1*, we then focused our in vitro and in vivo studies in mouse neuroglial progenitor cells on *Tsc2*. First, we show that shRNA-mediated knockdown (KD) of Tsc2 in vitro in mouse neural progenitor cells (mNPCs) leads to mTORC1 and mTORC2 activation, thus modeling human fetal brain tissue, and enhanced cell size that is prevented with the mTORC1 inhibitor rapamycin. We then show that Tsc2 shRNA KD in fetal mouse brains in vivo using in utero electroporation (IUE) causes aberrant cortical lamination that can be prevented with in utero rapamycin treatment. Our goal was to generate focal KD of Tsc2 to study the effects of Tsc2 loss on neural progenitor cells as well as on surrounding cells in the developing cortex.

Materials and Methods

Human TSC Fetal and Adult Tuber Specimens

Human fetal tuber specimens were obtained postmortem following fetal demise ($n = 4$; a twin pair, ages 23 weeks gestations, and single specimens at 34 and 38 weeks gestation) and the detection of tubers and subependymal nodule or cardiac rhabdomyoma (major diagnostic criteria for TSC) confirmed the diagnosis of TSC. The genotype of the 23-week twin pair was an identified *TSC2* mutation (2713C-T; R905W); mutation data was not available for the other human specimens. Control fetal brain specimens with normal cytoarchitecture ($n = 2$; age: 28 and 33 weeks gestation) were analyzed. Control adult brains were obtained post mortem. Adult TSC tuber specimens were obtained following surgical resection from 2 female TSC patients. For western analysis, control specimen was obtained postmortem (male; age: 28 years) and TSC tuber following surgical resection (male; age: 2 years).

Fixed, paraffin-embedded specimens, 5 sections per case, were probed with a panel of antibodies including P-p70S6K1 (T389; Cell Signaling), P-S6 (S235/236; Cell Signaling), c-myc (Abcam), P-PKCα (S657; Santa Cruz Biotechnology), P-SGK1 (S422; Santa Cruz Biotechnology), P-Akt (S473; Cell Signaling), P-NDRG1 (T346; Cell Signaling), and PKCα (Cell Signaling) overnight at 4 °C. Immunolabeling was visualized with avidin–biotin complex (Vectastain ABC Kit; Vector Labs) and 3,3′-diaminobenzidine (Sigma-Aldrich).

Cell Culture and Transfection

mNPCs derived from the subventricular zone (SVZ) of postnatal day 1 C57BL/6 mice (courtesy of Dr John Wolfe, Children's Hospital of Philadelphia, Philadelphia, PA, United States of America), were cultured on poly-D-lysine-coated plates in Dulbecco's modified Eagle medium: nutrient mixture F-12 supplemented with 1% fetal bovine serum, 1% N2 supplement, fibroblast growth factor, and heparin (Orlova, Parker et al. 2010). mNPCs express protein markers of a neuroglial progenitor state (SOX2, Nestin), and retain full differentiation capacity into neurons or astrocytes (Magnitsky et al. 2008; Orlova, Parker et al. 2010).

mNPCs were transfected with shRNA plasmids containing a green fluorescent protein (GFP) reporter under the control of a cytomegalovirus promoter (shRNA-GFP; SA Biosciences) targeting mouse Tsc2 or scrambled sequence (control) using Lipofectamine LTX/Plus Reagents (Invitrogen). shRNA constructs were commercially confirmed for absence of interferon response. In keeping with existing standards for shRNA experimentation in vitro and in vivo (Samuel-Abraham and Leonard 2010), multiple shRNA constructs to Tsc2 and scrambled sequence were tested. GFP-positive mNPCs were sorted using fluorescence-activated cell sorting (FACS) with a FACS Aria flow cytometer (BD Biosciences) at 2–5 days post transfection (DPT), plated and grown for 3–5 days, and used to generate protein lysates for western analysis. Rapamycin (100 nM; Cell Signaling) was added directly to cell culture media and administered for 24 h or daily for 5–7 days.

mNPCs lysates (radioimmunoprecipitation assay [RIPA] lysis buffer 50 mM Tris HCl, pH 8.0; 150 mM NaCl; 1% NP40; 0.5% sodium deoxycholate, 0.1% sodium dodecyl sulfate with protease and phosphatase inhibitors) separated on a 4–15% sodium dodecyl sulfate polyacrylamide gel electrophoresis gel (Bio-Rad), transferred onto polyvinylidene fluoride membranes and probed with Tsc2 (Abcam), phosphorylated 4E-BP1 (P-4E-BP1; T37/46; Cell Signaling), 4E-BP1 (Cell Signaling), P-S6 (S235/236; Cell Signaling), S6 (Cell Signaling), P-PKCα (S657; Santa Cruz Biotechnology), PKCα (Cell Signaling), P-Akt (S473; Cell Signaling), Akt (Cell Signaling), P-NDRG1 (T346; Cell Signaling), NDRG1 (Abcam) antibodies overnight at 4 °C, and horseradish peroxidase-conjugated secondary antibodies (GE Healthcare) for 1 h at room temperature, and visualized with ECL or ECL Plus (GE Healthcare). Membranes were probed with antibodies to glyceraldehyde-3-phosphate dehydrogenase (GAPDH) (Cell Signaling) to ensure equal protein loading.

In Utero Electroporation and Rapamycin Administration

Animal experiments were approved by the Institutional Animal Care and Use Committee of the University of Pennsylvania.

Time-pregnant C57BL/6J mice at embryonic day 14 (E14) were placed under isoflurane-induced anesthesia, and the uterine horns were surgically exteriorized. shRNA-GFP plasmids targeting mouse Tsc2 or control scrambled sequence (3–8 μg/μL) diluted in TE Buffer (Qiagen) and fast green dye (0.3 mg/mL; Sigma-Aldrich) were microinjected through the uterine wall into one lateral ventricle of each embryo. Tsc2 shRNA clone #4 was used for IUE experiments. Five electrical pulses (40 V, 50-ms duration, 1000-ms intervals) (Saito 2006) were delivered across the embryonic head using CUY21 Edit Square Wave Electroporator (Nepagene). Uterine horns were returned to the pelvic cavity and the abdominal wall was closed by suture. Females were returned to the cage and embryos were sacrificed 5 days later at E19.

BrdU (50 mg/kg body weight) was intraperitoneally injected at E14. Rapamycin (0.5, 2.5, or 5.0 mg/kg body weight) diluted in vehicle solution (5% PEG 400, 5% Tween 80, and 0.9% NaCl/H_2O) was intraperitoneally injected daily for 4 days (E15-E18) or 5 days (E14-E18).

Fixed, cryoprotected embryonic mouse brains were cryostat sectioned at 20 μm thickness. Sections were probed with antibodies to P-S6 (S235/236; Cell Signaling; Bethyl Laboratories), Cux1 (Santa Cruz Biotechnology), Ctip2, Tbr1, MAP2 (Abcam), and BrdU (Millipore). Sections were subsequently stained with Texas Red (Vector Labs), Cy3, Cy5 (Jackson Immunoresearch), AlexaFluor647 (Invitrogen) secondary antibodies, and Hoechst33342 (0.0001 μg/μL; Invitrogen) to visualize cell nuclei and define the zones of the embryonic brain based on cellular density. Fluoromount-G (SouthernBiotech) mounting media was used to mount the sections.

Quantitative Analysis

Cell size was compared by FACS sorting mNPCs transfected with scrambled or Tsc2 shRNA-GFP plasmids for GFP. The scrambled and Tsc2 shRNA-transfected mNPCs were sorted using the same parameters and consecutively during one run. Forward scatter area (FSC-A) and side scatter area (SSC-A) histograms for scrambled and Tsc2 GFP-positive cell populations were compared. Mean and standard deviation were computed for FSC-A and SSC-A measurements and compared using one-way ANOVA ($P < 0.05$).

Total cell area of mNPCs was quantified in digital images (Leica DMI6000B microscope and Leica DFC360FX camera) by outlining the cell circumference of GFP-positive cells and utilizing the ImagePro Plus software (Media Cybernetics) area measurement function. Cell area measurements were compared between control, scrambled shRNA-, and Tsc2 shRNA-transfected mNPCs in untreated, vehicle (DMSO), and rapamycin (100 nM) treated conditions (one-way ANOVA, Tukey–Kramer post hoc analysis for multiple comparisons; $P < 0.05$).

The laminar position of shRNA-transfected cells in vivo was assessed at E19 in homologous cortical regions ($n = 5$ embryos per condition; 3–8 rostral to caudal sections per embryo were analyzed). GFP-positive cells were identified in a focal region in frontal cortex anterior to the rostral hippocampus. The zones of the developing embryonic brain: ventricular zone (VZ)/SVZ, intermediate zone (IZ), and cortical plate (CP), were defined by the density of Hoechst-positive nuclei. The CP region was split into 3 equal segments: lower CP (LW_CP), middle CP (MID_CP), and upper CP (UP_CP), for further quantification. A region of interest (ROI) spanning these zones was delineated by a rectangle extending from the pial surface to the lateral ventricle that circumscribed the transfected region. The total number of transfected GFP-positive cells quantified was approximately equal for each experimental group. The number of GFP-positive cells within each zone and in the ROI was counted in a blinded fashion in 3–8 sections spanning rostral to caudal regions for each animal. The data were expressed as the percentage of total GFP-positive cells in a given ROI located in each defined zone ± standard error of the mean (SEM; GraphPad Prism software, one-way ANOVA, Dunnett's post hoc analysis for multiple comparisons $P < 0.05$) (Nguyen et al. 2006).

Quantification of Cux1-positive cells surrounding the area of GFP-positive cells was conducted by calculating the density of Cux1-positive cells in each individual section (# of cells/ ROI area). ROI encompassed the area of GFP-positive cells spanning IZ, LW_CP, and MID_CP regions. The average ROI area was 235550 μm^2. The density

was then multiplied by the average ROI area and the numbers were statistically compared across different conditions. The data were expressed as total number of Cux1-positive cells in normalized ROI ± standard error of the mean (SEM; GraphPad Prism software, one-way ANOVA and Tukey's post hoc analysis for multiple comparisons, $P < 0.05$).

Results

Activation of mTOR Pathway in Human Fetal TSC Brain

Histological analysis of fetal TSC tissue ($n = 4$) revealed isolated regions of cell clusters exhibiting disorganized lamination and multiple enlarged cells reminiscent of pathology in surgically resected tubers in pediatric and adult patients. Indeed, the detection of altered cortical lamination and enlarged cells supported a pathological diagnosis of tubers similar to the one described previously in a 20-week gestation TSC fetus (Park et al. 1997). Fetal TSC tuber tissue exhibited robust P-p70S6K1 (T389) and P-S6 (S235/236) expression, especially in enlarged cells, which correlated with the expression pattern in adult TSC tubers (Fig. 1). While quantitative comparison of mTOR substrates in each fetal specimen and the adult specimens was limited by our sample size,

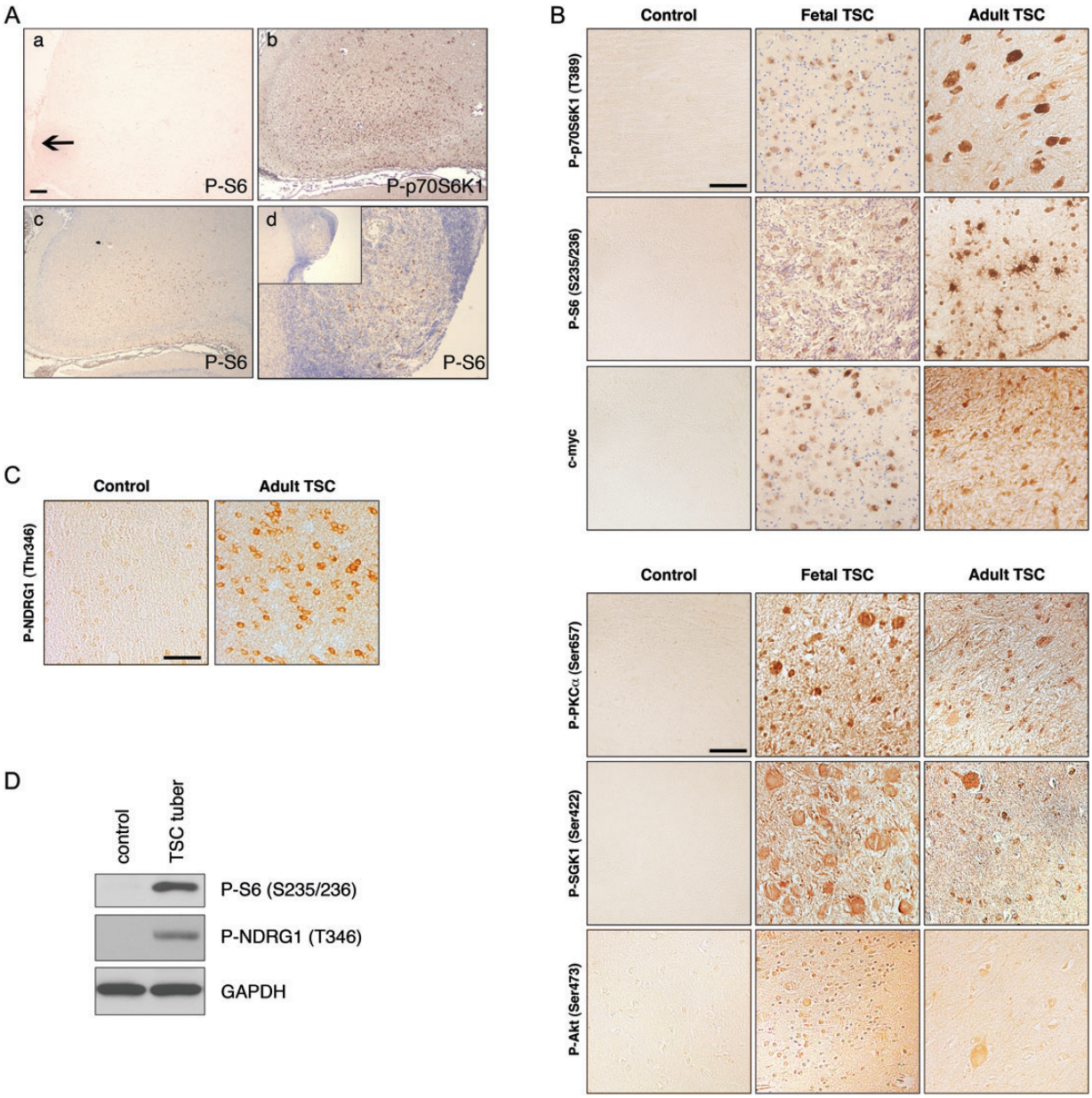

Figure 1. mTORC1 and mTORC2 signaling pathway activation in fetal and adult TSC brains. (*A*) Control and fetal TSC tuber specimens. (a) Absence of P-S6 (S235/236) immunolabeling in control fetal brain (arrow depicts cortical surface). (b and c) Robust P-p70S6K1 (T389) and P-S6 (S235/236) in fetal TSC tuber. (d) P-S6 (S235/236) expression in fetal TSC subependymal nodule specimen. Inset, low magnification image. Scale bar: 200 μm. (*B*) mTORC1 signaling pathway activation in fetal and adult tubers, with robust immunoreactivity for P-p70S6K1 (T389), P-S6 (S235/236), and c-myc. mTORC2 signaling pathway activation in fetal and adult TSC tubers, with robust immunoreactivity for P-PKCα (S657), P-SGK1 (S422), and P-Akt (S473). Scale bar: 50 μm. (*C*) P-NDRG1 (T346) immunoreactivity was robust in adult TSC brain specimens compared with controls. Scale bar: 50 μm. (*D*) Western assay of human control and TSC tuber specimens. Increased levels of P-S6 (S235/236) and P-NDRG1 (T346) were observed in TSC tuber case compared with control brain. glyceraldehyde-3-phosphate dehydrogenase (GAPDH) was used as a loading control.

overall it appeared qualitatively that phospho-protein expression was more robust in adult tubers compared with early fetal (23 week) tissue but differences between fetal specimens could not be appreciated. In the monozygotic twins specimens, the extent of mTOR activation did not differ within specimens. In one fetal case, a subependymal nodule was available for analysis and exhibited P-p70S6K1 (T389) and P-S6 (S235/236) immunoreactivity (Fig. 1*A*). We have previously demonstrated that c-myc, a downstream transcriptional activator of mTORC1, is expressed in surgically resected cortical tubers (Orlova, Tsai et al. 2010). C-myc was detected in fetal TSC tuber specimens in a pattern similar to P-p70S6K1 and P-S6 (Fig. 1*B*). Analysis of mTOR activation in control fetal brain specimens ($n = 2$) did not reveal immunoreactivity for P-p70S6K1 (T389), P-S6 (S235/236), or c-myc. Furthermore, fetal and adult TSC tuber tissue was evaluated for mTORC2 immunoreactivity. P-PKCα (S657), P-SGK1 (S422), and P-Akt (S473) have been established as biomarkers for mTORC2 signaling pathway activation (Guertin and Sabatini 2007). Phosphorylation of SGK1 at S422 results in activation of SGK1 and phosphorylation of its effector NDRG1 (T346) (Garcia-Martinez and Alessi 2008). Robust immunoreactivity for P-PKCα (S657), P-SGK1 (S422), and P-Akt (473) was detected in fetal TSC tuber specimens, and immunoreactivity for P-PKCα (S657), P-SGK1 (S422), P-Akt (S473), and SGK1 substrate, P-NDRG1 (T346), was detected in adult TSC tuber cases (Fig. 1*B-D*). P-PKCα (S657), P-SGK1 (S422), P-Akt (S473), and P-NDRG1 (T346) immunohistochemical staining was virtually absent in control specimens (Fig. 1*B*,*C*). Expression of the native PKCα isoform was the same in adult TSC and control brain tissue (Supplementary Fig. 1). These findings demonstrate for the first time that there is mTORC1 signaling activation in fetal tubers, and that in addition to mTORC1 activation, there is mTORC2 activation in fetal and adult TSC brains. As in adult TSC brains (Marcotte et al. 2012), specimens of perituberal cortex with normal cytoarchitecture in fetal cases do not demonstrate evidence of mTOR hyperactivation (see cortex surrounding the fetal tubers, Fig. 1*A*).

Depletion of Tsc2 and Activation of mTOR in mNPCs In Vitro

It is speculated by many investigators that tubers form because of the effects of loss of *TSC1* or *TSC2* on neural progenitors in the fetal human cortex. Thus, to investigate the effects of Tsc2 loss in neural progenitor cells, mNPCs were transfected with 3 different shRNA constructs targeting disparate regions of Tsc2 mRNA or a scrambled sequence not recognizing any known mouse mRNA as a control (Supplementary Fig. 1).

At 4–10 DPT, Tsc2 shRNA-GFP clone #1 (5′-GCATGCAGTT CTCACCTTATT-3′), clone #3 (5′-AGAGCTGTCCAATGCCCTTA T-3′) and clone #4 (5′-GAAGGATTTCGTCCCTTATAT-3′) resulted in reproducible Tsc2 KD (Supplementary Fig. 1). Semiquantitative densitometric analysis estimated Tsc2 KD at

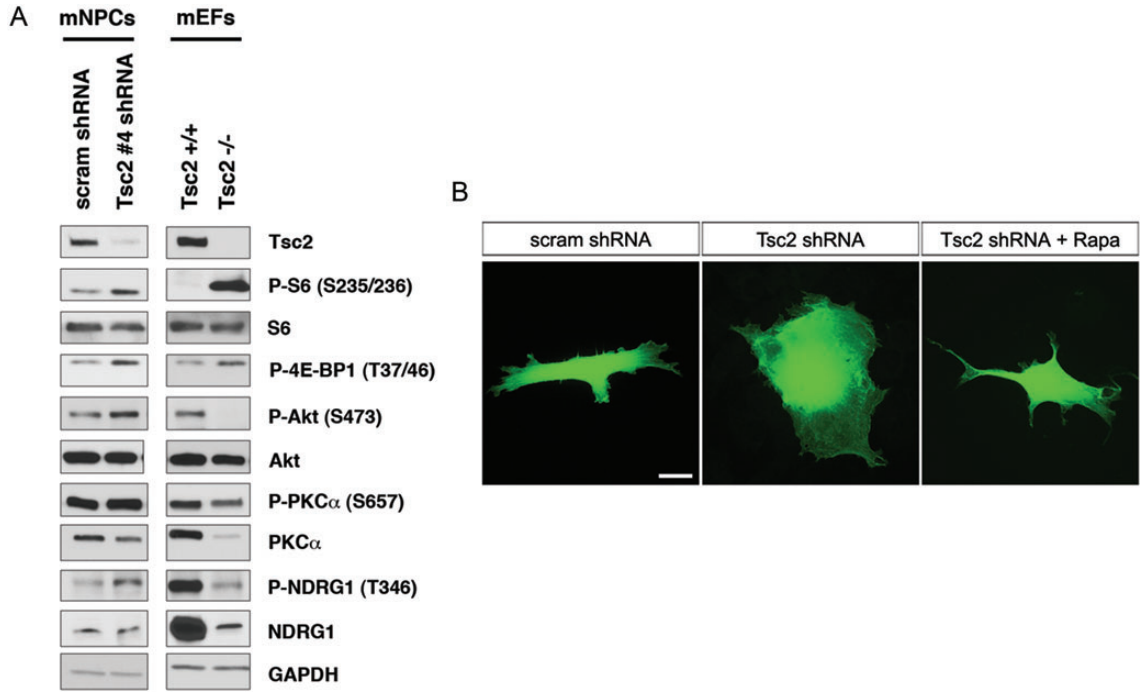

Figure 2. Tsc2 shRNA KD in mNPCs results in mTORC1 and mTORC2 pathway activation and increased cell size in vitro. (*A*) Western blot depicting reduced Tsc2 protein levels following Tsc2 shRNA KD in mNPCs with Tsc2 shRNA-GFP clone #4 at 4-10 DPT. Tsc2 shRNA-GFP clone #4 resulted in the highest level of Tsc2 KD and semiquantitative densitometric analysis estimated it at 40–70%. Tsc2 shRNA KD in mNPCs leads to increased P-S6 (S235/236) and P-4E-BP1 (T37/46) levels as a consequence of mTORC1 pathway activation compared with scrambled shRNA-GFP control. Total S6 and 4E-BP1 levels were unchanged (in addition see Supplementary Fig. 1). Similar results were observed in $Tsc2^{-/-}$ mEFs, with increased P-S6 (S235/236) and P-4EBP1 (T37/46), compared with $Tsc2^{+/+}$ mEFs. KD of Tsc2 shRNA in mNPCs also resulted in increased levels of P-Akt (S473), P-PKCα (S657), and P-NDRG1 (T346), which are biomarkers of mTORC2 signaling activation. These results were opposite of the pattern observed in $Tsc2^{+/+}$ and $Tsc2^{-/-}$ mEFs, as $Tsc2^{-/-}$ mEFs show decreased mTORC2 signaling (decreased levels of P-Akt (S473), P-PKCα (S657), and P-NDRG1 (T346)), compared $Tsc2^{+/+}$ mEFs. GAPDH was used as a loading control. (*B*) mNPCs transfected with Tsc2 shRNA-GFP clone #4 ($n = 20$) exhibit a 1.9-fold increase in total cell area compared with scrambled shRNA-GFP transfected control cells ($n = 17$; $P < 0.01$). Rapamycin (100 nM) treatment rescued cell size enhancement with cell area being approximately the same size as vehicle-treated and untreated scrambled shRNA-GFP transfected control mNPCs ($n = 21$; $P < 0.05$).

~40–70% for all 3 shRNAs. Tsc2 shRNA clone #1 and #4 were chosen for subsequent in vitro mNPC experiments. Tsc2 shRNA clone #1 and #4 showed enhanced mTORC1 signaling in mNPCs as evidenced by increased levels of P-S6 (S235/236) and P-4E-BP1 (T37/46); native levels of these proteins did not change (Fig. 2*A* and Supplementary Fig. 1). Furthermore, Tsc2 shRNA KD resulted in mTORC2 signaling pathway activation as evidenced by increase in levels of P-Akt (S473) and P-NDRG1 (T346) compared with scrambled shRNA-transfected controls (Fig. 2*A*). Total (nonphosphorylated isoforms) for Akt and NDRG1 did not change; however, PKCα levels following KD were decreased compared with controls.

Previous studies have demonstrated that mTORC2 activation is diminished in mouse embryonic fibroblasts (mEFs) lacking *Tsc2* (Huang et al. 2008). In keeping with these results, we also found decreased mTORC2 activity in *Tsc2* null ($Tsc2^{-/-}$) mEFs, as evidenced by decreased levels of P-PKCα (S657), P-Akt (S473), P-NDRG1 (T346) compared with $Tsc2^{+/+}$ controls (Fig. 2*A*; courtesy of Dr Elizabeth Henske, Dana Farber Cancer Center, Boston, MA, United States of America). Thus, our results in fetal brain tissue and mNPCs showing enhanced mTORC2 activation suggest a specific signaling effect in neural progenitor cells distinct from other cell types.

Tsc2 Regulation of mNPC Size is Rapamycin-Dependent

At 4–10 DPT, Tsc2-depleted mNPCs were FACS sorted and showed increased forward scatter area (FSC-A), which is a measurement reflective of cell size (Fingar et al. 2002). The mean FSC-A of Tsc2 shRNA-transfected mNPCs ($n = 7379$) was significantly greater than mean FSC-A of scrambled shRNA-transfected mNPCs ($n = 4681$; $P < 0.05$; Supplementary Fig. 1). As the FSC-A is a relative measure between different experimental groups, fluorescent images were acquired of individual cells, and the cell area, defined by the GFP fluorescence, was compared for scrambled shRNA control and Tsc2 shRNA-transfected mNPCs (Fig. 2*B*). Tsc2-depleted mNPCs ($n = 20$) had cell area twice the size of scrambled shRNA control mNPCs ($n = 17$; $P < 0.01$). No change in cell area was found following administration of transfection reagents alone, as previously reported (Orlova, Parker et al. 2010).

To determine whether increased cell size was mTORC1 dependent, control scrambled shRNA and Tsc2-depleted mNPCs were treated with the mTORC1 inhibitor rapamycin. Rapamycin (100 nM) application for 24 h had no significant effect on the cell size of wild-type or scrambled shRNA-GFP-transfected mNPCs, as has been previously reported (Orlova, Parker et al. 2010). However, rapamycin treatment prevented cell size enlargement in Tsc2-depleted cells and mean FSC-A of rapamycin-treated Tsc2 shRNA KD cells ($n = 7353$) was similar to control scrambled shRNA cells (Supplementary Fig. 1). Rapamycin prevented cell area increase of Tsc2 shRNA-transfected mNPCs ($n = 21$; $P < 0.05$), and the rapamycin-treated Tsc2 KD mNPCs had approximately the same cell area as scrambled shRNA mNPCs (Fig. 2*B*). Thus, Tsc2 depletion in mNPCs results in enhanced cell size that is preventable by treatment with rapamycin, suggesting an mTORC1-dependent mechanism.

Tsc2 Depletion In Vivo Results in a Cortical Malformation

To investigate the effects of TSC2 in vivo on cortical development, we transfected Tsc2 shRNA-GFP into embryonic mouse brains by IUE at embryonic day 14 (E14) (Saito 2006) and assessed the effects on migration and lamination at E19 (Fig. 3*A*). Scrambled shRNA-GFP plasmids were electroporated in a parallel set of experiments as controls for IUE and shRNA transfection.

By E19, GFP-positive cells transfected with control-scrambled shRNA-GFP plasmid were primarily localized in the upper region of the CP (UP_CP 67.3 ± 1.3%) and a small number of transfected progenitors remained in VZ/SVZ (18.6 ± 1.9%; Fig. 3*B*). In contrast, following transfection with Tsc2 shRNA-GFP, there were significantly fewer GFP-positive cells that reached the upper CP region (Tsc2 shRNA-GFP UP_CP 19.1 ± 3.4%; $P < 0.05$ compared with scrambled shRNA-GFP controls), and there was an increase in the number of GFP-positive cells found in the VZ/SVZ region (37.6 ± 1.9%; $P < 0.05$, compared with scrambled shRNA-GFP controls). Furthermore, very few scrambled shRNA-GFP cells were found in the IZ (4.6 ± 1.0%), lower- (LW_CP; 3.8 ± 0.8%) or middle (MID_CP; 5.8 ± 1.3%) cortical plate, whereas significantly more Tsc2-depleted GFP-positive cells were found in those regions (IZ 16.8 ± 2.37%, LW_CP 12.1 ± 2.8%, MID_CP 14.3 ± 1.0%). Tsc2 shRNA KD led to a focal cortical malformation with fewer cells reaching their appropriate cortical laminar destination (UP_CP, layers II–III) and the majority of cells found in the VZ/SVZ, IZ, LW_CP, and MID_CP (Fig. 3*B*). Immunohistochemical staining with MAP2 showed that cells which leave the VZ/SVZ in Tsc2 shRNA condition express MAP2 and appear to take on a neuronal phenotype (Fig. 3*C*).

Tsc2 Depletion Results in Increased Cell Volume In Vivo

To investigate whether Tsc2 depletion results in cytomegaly in vivo, we acquired *z*-stack images of GFP-positive cells using confocal microscopy. Cell volume was measured by defining the volume encompassed by the GFP fluorescence signal. Quantitative analysis revealed that GFP-positive Tsc2 shRNA cells in the IZ had approximately twice the volume (408.4 μm^3) of scrambled shRNA control cells in the UP_CP (267.7 μm^3), and some exhibited the morphology reminiscent of giant cells, with a laterally displaced nucleus as seen in human TSC tuber specimens (Fig. 3*D*, also see Supplemental videos in Supplementary Figs. 2 and 3).

Tsc2 KD In Vivo Results in Cell-Autonomous and Non-Cell-Autonomous Lamination Defects of Layers II–III

To confirm the laminar destination of electroporated cells, sections were stained with homeobox transcription factor Cux1 which labels cells in superficial cortical layers II–III born on approximately E14–15 (Fig. 4*A*) (Nieto et al. 2004). Cux1-immunolabeling in scrambled shRNA condition revealed a band of cells primarily confined to the superficial part of the CP (layers II–III), thus IUE or plasmid transfection conditions alone did not alter normal cortical development or affect migration of cells destined for layers II–III of the cortex (Fig. 4*A*,*B*). Scrambled shRNA GFP-positive cells colocalized with Cux1-labeled cells in layers II–III at E19 and expressed Cux1 (100%; $n = 16$) (Fig. 4*A*). Conversely, only 21% of GFP-positive cells following IUE with Tsc2 shRNA were Cux1-positive, while the majority (79%) were Cux1-negative ($n = 14$) (Fig. 4*A*). Interestingly, while most Tsc2 shRNA

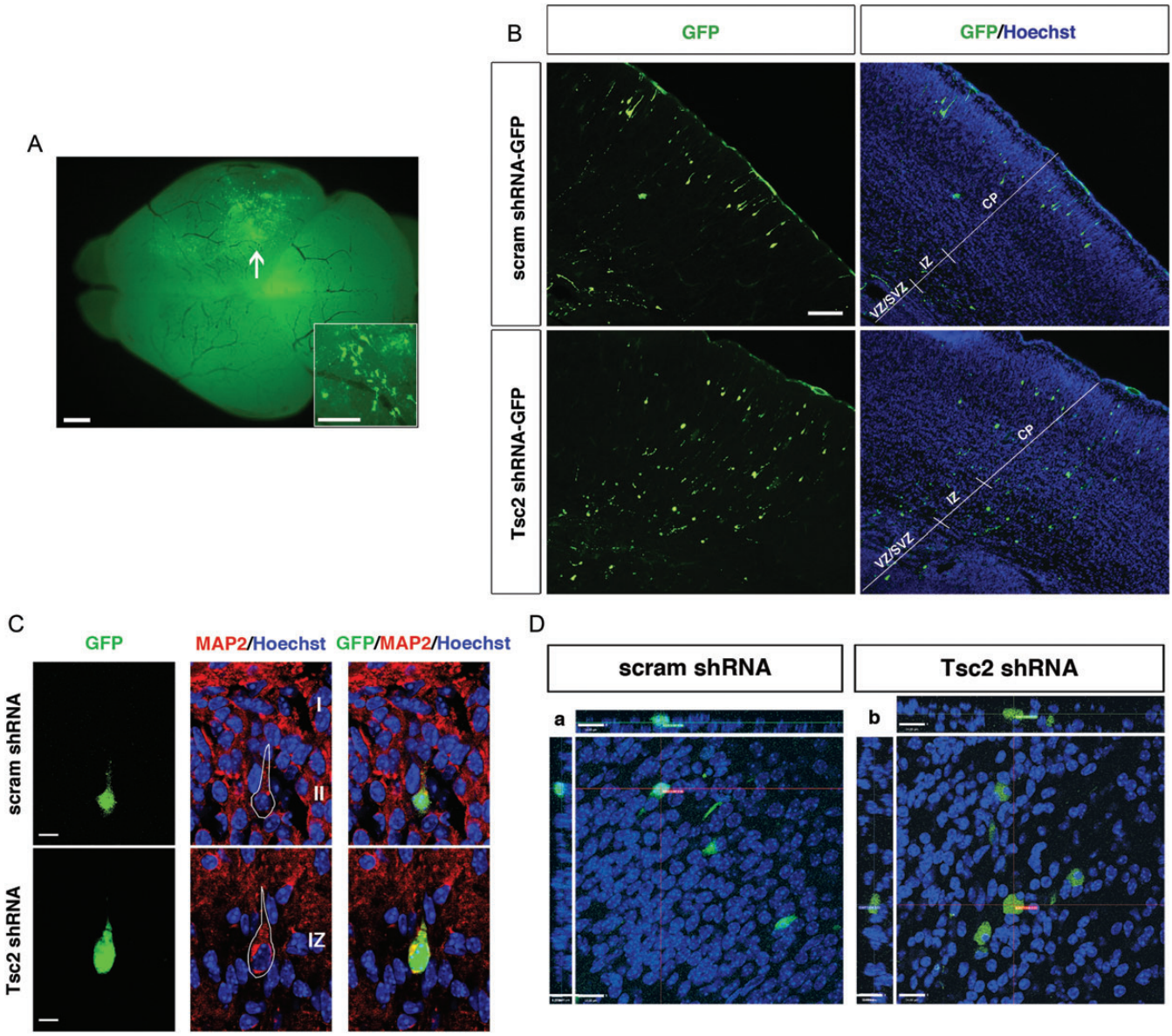

Figure 3. Focal Tsc2 shRNA KD results in a cortical malformation and cytomegaly in vivo. (*A*) Whole brain green fluorescent protein (GFP) fluorescence image demonstrating focal area of cell transfection (arrow) following in utero electroporation with Tsc2 shRNA-GFP plasmid. Inset is a higher power magnification image showing GFP-expressing cells. Scale bar: 500 μm; Inset scale bar: 100 μm. (*B*) (Top) E19 brain transfected with control scrambled shRNA-GFP at E14, with the majority of GFP-positive cells reaching their appropriate destination in the upper region of cortical plate (layers II–III). (Bottom) E19 brain transfected with Tsc2 shRNA-GFP at E14. In vivo Tsc2 shRNA KD resulted in a focal lamination defect with the majority of cells localized in the VZ and IZ, and few reaching their appropriate destination in the upper region of cortical plate (layers II–III). For quantification, see text and Figure 5. Scale bar: 100 μm. (*C*) MAP2 immunostaining of IUE E14-19 scrambled shRNA-GFP and Tsc2 shRNA-GFP brains. (Top) Control scrambled shRNA GFP-positive cells in layers II–III express neuronal marker MAP2. (Bottom) Tsc2 shRNA GFP-positive cells that leave VZ/SVZ, but do not reach their layers II–III cortical destination, also express MAP2 (image shown of cell located in the IZ). Hoechst33342 was used to visualize cell nuclei. Scale bar: 7 μm. (*D*) Confocal images of IUE E14-19 (a) scrambled shRNA-GFP and (b) Tsc2 shRNA-GFP transfected cells in layers II–III and IZ, respectively. Tsc2 shRNA KD results in cell volume increase (cytomegaly), compared with scrambled shRNA-GFP control cells. For quantification, see text and Figure 5. Scale bar: 14 μm.

GFP-positive cells were Cux1-negative, we noticed that there was an increase in Cux1-labeling in cells surrounding GFP-positive cells in IZ and lower CP regions below layers II–III (Fig. 4*B*). To verify that this was not a result of IUE, we compared the density of Cux1-labeled cells in the ROI surrounding the GFP-positive in scrambled shRNA condition, to density in the contralateral non-electroporated hemisphere (Supplementary Fig. 4). There was no statistical significance between the counts on the electroporated GFP-positive hemisphere and non-electroporated hemisphere in scrambled shRNA condition (Supplementary Fig. 4). To compare the counts in the scrambled shRNA and Tsc2 shRNA conditions, density in ROI of equal size was normalized to non-electroporated hemisphere as an internal control. The ratios were further normalized to scrambled shRNA counts and revealed that there was a 2-fold increase in the number of non-transfected Cux1-labeled cells surrounding the GFP-positive cells in IZ, LW_CP, and MID_CP in Tsc2 shRNA condition compared with scrambled shRNA controls (Fig. 4*B*; $P < 0.05$). These results suggest both cell-autonomous effects of Tsc2

KD on migration, as well as non-cell-autonomous lamination effects on the surrounding neighboring cells.

To test the effects of Tsc2 KD on neighboring cells in other cortical layers, we immunohistochemically labeled for Ctip2 and Tbr1, which are layer V and layer VI markers (Hevner et al. 2001; Arlotta et al. 2005; Chen et al. 2005; Molyneaux et al. 2005). In the scrambled shRNA-GFP control condition, virtually all cells that migrated into the CP reached layers II–III, above the band of Tbr1- and Ctip2-labeled cells (Fig. 4*C*). On the other hand, in the Tsc2 shRNA KD condition, majority of GFP-positive cells were localized to the VZ/SVZ, IZ and lower regions of the CP (LW_CP, MID_CP). As mentioned previously, only 21% of GFP-positive Tsc2 shRNA-transfected cells were Cux1-positive and thus we wanted to evaluate

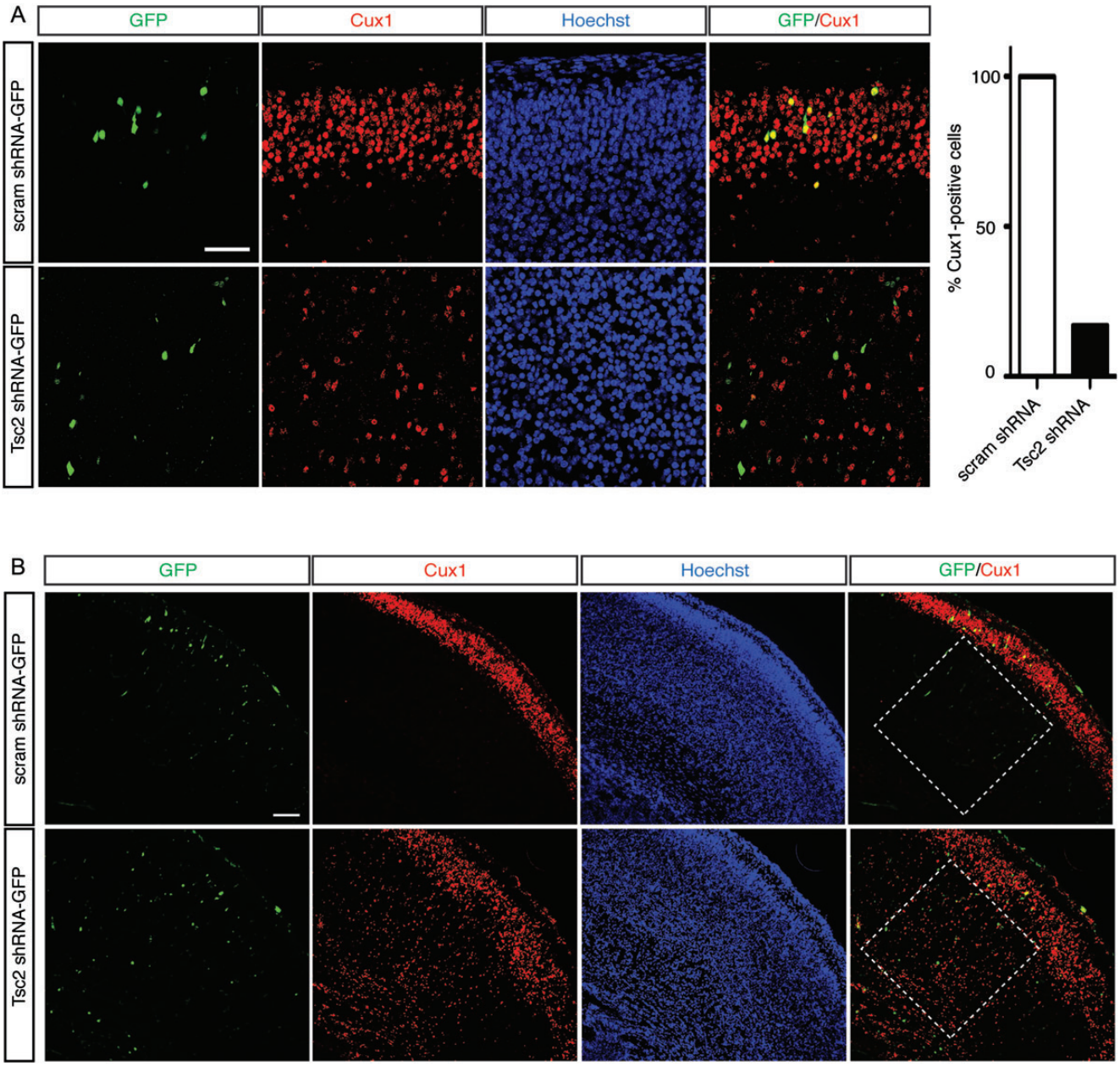

Figure 4. In vivo Tsc2 shRNA KD results in cell-autonomous and non-cell-autonomous lamination defect. (*A*) IUE E14-19 scrambled shRNA-GFP and Tsc2 shRNA-GFP brains immunostained with a layer II–III marker Cux1. Scrambled shRNA GFP-positive cells co-localize with Cux1-immunoreactive cells in layers II–III at E19, and are Cux1-positive. In contrast, majority of Tsc2 shRNA KD GFP-positive cells, which did not reach their appropriate cortical destination (layers II–III), are Cux1-negative (79%). Quantification graph of GFP-positive cells analyzed by confocal microscopy in scrambled shRNA and Tsc2 shRNA brains, showing that 100% of cells in scrambled shRNA-GFP condition in layers II–III expressed Cux1, however only 21% of GFP-positive cells in Tsc2 shRNA KD condition were Cux1-positive. (scrambled shRNA-GFP $n = 16$ cells, Tsc2 shRNA-GFP $n = 14$ cells; 3 embryonic brains per condition were analyzed). Scale bar: 50 μm. (*B*) Non-cell-autonomous effects of Tsc2 shRNA KD on surrounding Cux1-positive cells. In the scrambled shRNA condition, there was a tight band of Cux1-positive cells (layers II–III) in the superficial region of the cortical plate. Very few Cux1-positive cells were noted in the ROI spanning the IZ, LW_CP, and MID_CP (white box). However, in the ROI surrounding the GFP-positive cells in Tsc2 shRNA KD condition, there was a significant increase in Cux1-positive cells. For quantification, see text and Figure 5. Scale bar: 100 μm. (*C*) Confocal images of IUE E14-19 scrambled shRNA-GFP and Tsc2 shRNA-GFP brains immunostained with deep layers V and VI, markers Ctip2 and Tbr1, and neuronal marker MAP2. Hoechst33342 was used to visualize cell nuclei. Tsc2 shRNA KD cells, which do not reach their appropriate cortical layer II–III destination, do not acquire identity of other cortical layers (e.g., V and VI). Scale bar: 100 and 50 μm (left to right).

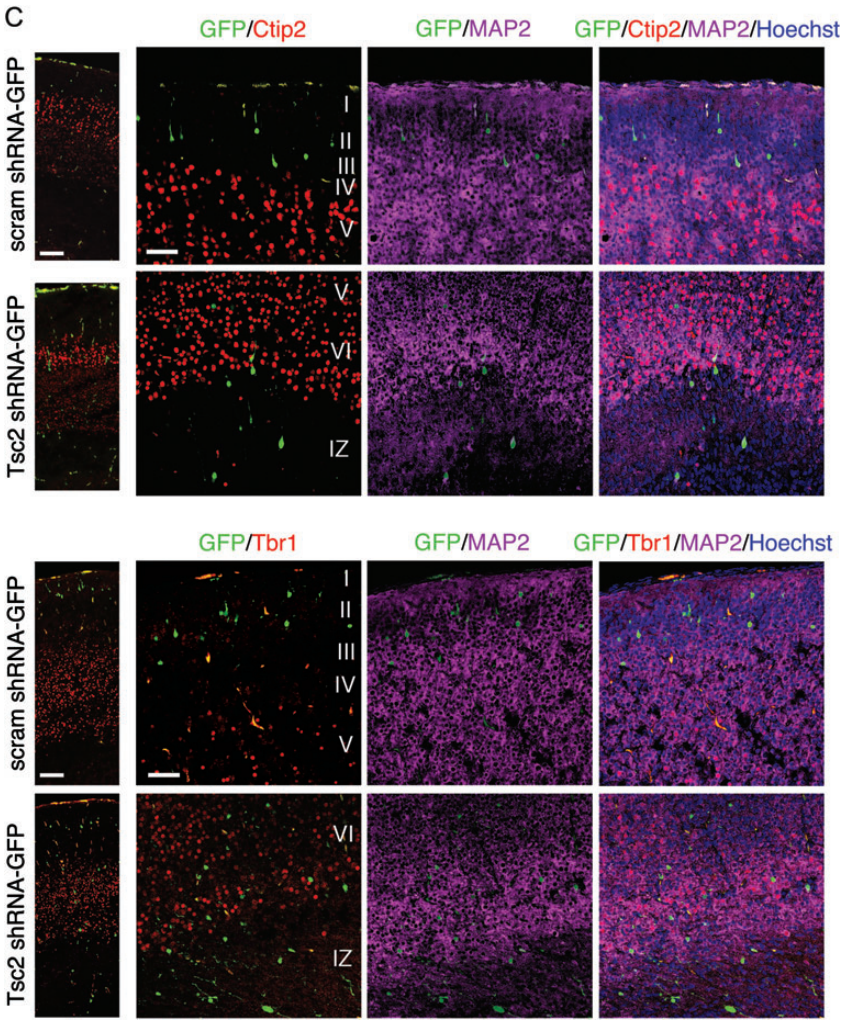

Figure 4. Continued

whether these cells that do not appropriately migrate do so because of expression of other layer-specific markers, such as Tbr1 and Ctip2. E19 sections were imaged by confocal microscopy and revealed that the Tsc2 shRNA GFP-positive cells in the IZ were Ctip2- and Tbr1-negative (Fig. 4*C*). To further investigate whether the Tsc2 shRNA GFP-positive cells that migrated into the CP, but did not reach layers II–III, assume the identity of a different cortical layer (e.g., layer V or VI), we looked at their Ctip2 and Tbr1 expression pattern. Tsc2 shRNA GFP-positive cells in the LW_CP and MID_CP were MAP2-positive, and Ctip2- and Tbr1-negative, indicating that at least at E19, they do not express layers V and VI markers Tbr1 and Ctip2 and thus, likely do not acquire layer V or VI identity (Fig. 4*C*).

Migratory Defect Following Tsc2 KD is Prevented with Rapamycin Treatment

Enhanced P-S6 levels in cells transfected with Tsc2 suggested that the induced cortical lamination defect could be dependent on the hyperactive mTORC1 signaling. Mean P-S6 labeling intensity was measured, normalized to background, and demonstrated a 2-fold increase in P-S6 in Tsc2 shRNA-transfected cells compared with scrambled shRNA-transfected controls ($n = 20$, $P < 0.05$; Fig. 5*B*). To test this hypothesis, we administered rapamycin daily to the pregnant dam between E15-E18. Rapamycin treatment (2.5, 5.0 mg/kg body weight) led to near complete inhibition of mTOR signaling in liver (absent P-S6 levels) compared with vehicle or low dose (0.5 mg/kg) rapamycin at E19 (see Supplementary Fig. 5). In the brain, rapamycin (5.0 mg/kg) prevented the migratory defect of GFP-positive cells transfected with Tsc2 shRNA (Fig. 5A). Rapamycin treatment resulted in a 2-fold increase in the number of GFP-positive Tsc2 shRNA-transfected cells reaching the upper CP layers (UP_CP $46.5 \pm 4.8\%$; $P < 0.05$ compared with untreated Tsc2 shRNA condition) and approximately a 2-fold decrease of transfected cells remaining within VZ/SVZ ($21.0 \pm 1.5\%$; $P < 0.05$ compared with untreated Tsc2 shRNA condition) compared with vehicle-treated animals (UP_CP $19.1 \pm 3.4\%$, VZ/SVZ $37.6 \pm 1.9\%$; Fig. 5*A*). In addition, no change was noted in the lamination pattern of the surrounding cortex either ipsi- or contralateral to the induced malformation (data not shown). Consistent with these findings, confocal fluorescence microscopy and immunodensitometry demonstrated that rapamycin treatment reduced P-S6 levels in the Tsc2 shRNA-GFP-transfected cells to near baseline ($P > 0.05$ compared with control scrambled shRNA-GFP; Fig. 5*B*).

To test whether rapamycin alone altered normal cortical migration, we injected BrdU at E14 and administered

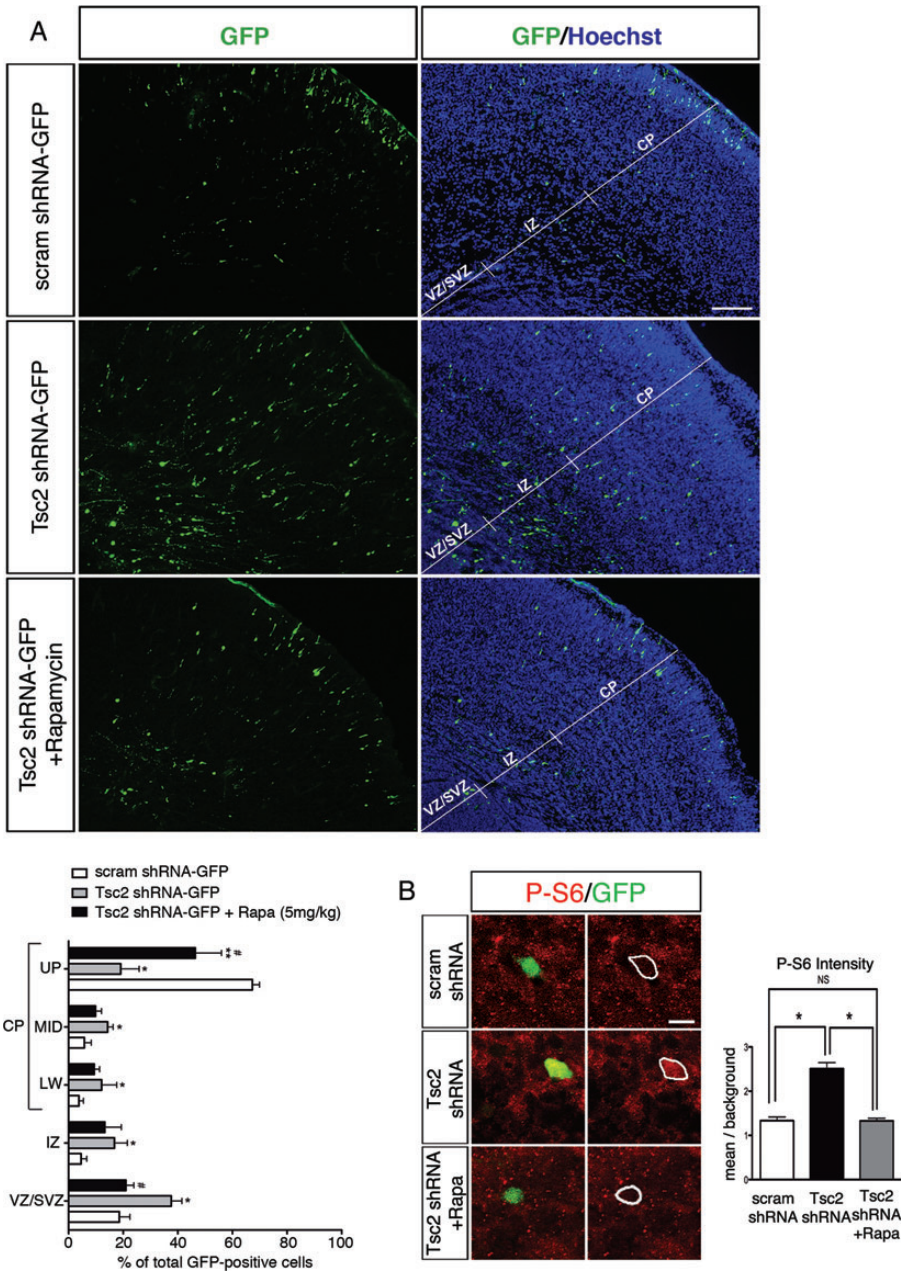

Figure 5. Fetal rapamycin treatment rescues the lamination defect, cytomegaly and non-cell-autonomous lamination effects following Tsc2 shRNA KD in vivo. (*A*) (Top) Scrambled shRNA-GFP transfected cells at E14 laminate layers II–III of the cortex at E19 (UP_CP 67.3 ± 1.3%, MID_CP 5.8 ± 1.3%, LW_CP 3.8 ± 0.8%, IZ 4.6 ± 1.0%, VZ/SVZ 18.6 ± 1.9%). (Middle) Tsc2 shRNA-GFP KD at E14 leads to a lamination defect with cells abnormally retained in the VZ/SVZ, IZ, and LW_CP at E19 as compared with scrambled shRNA-GFP controls (UP_CP 19.1 ± 3.4%, MID_CP 14.3 ± 1.0%, LW_CP 12.1 ± 2.8%, IZ 16.8 ± 2.4%, VZ/SVZ 37.6 ± 1.9%; $P < 0.05$). (Bottom) With daily rapamycin treatment (5.0 mg/kg body weight) for 4 days (E15–E18), a significantly greater number of Tsc2 shRNA-GFP KD cells reach their appropriate destination layers II–III of the cortex (UP_CP 46.4 ± 4.8%; $P < 0.05$), and fewer are retained in the VZ/SVZ (21.0 ± 1.5%; $P < 0.05$). (MID_CP 9.9 ± 1.1%, LW_CP 9.4 ± 1.0%, IZ 13.3 ± 3.0%). Graphic representation of the percentage of GFP-positive cells in each region: VZ/SVZ, IZ, LW_CP, MID_CP, and UP_CP of the total GFP-positive cells in scrambled shRNA-GFP, Tsc2 shRNA-GFP, and rapamycin-treated Tsc2 shRNA-GFP conditions. *Tsc2 shRNA-GFP versus scram shRNA GFP ($P < 0.05$); **rapamycin-treated (5.0 mg/kg body weight; E15-E18) Tsc2 shRNA-GFP versus scram shRNA GFP ($P < 0.05$); # rapamycin-treated (5.0 mg/kg body weight; E15-E18) Tsc2 shRNA-GFP versus Tsc2 shRNA-GFP ($P < 0.05$). Scale bar: 100 μm. (*B*) Tsc2 shRNA KD in vivo results in mTORC1 hyperactivation that is rescued with rapamycin treatment. (Top) P-S6 (S235/236) immunolabeling in scrambled shRNA-GFP-transfected cells. (Middle) Following Tsc2 shRNA KD there was a marked 2-fold increase in P-S6 intensity compared with scrambled shRNA controls. (Bottom) Daily treatment with rapamycin (E15-E18) prevented mTORC1 hyperactivation following Tsc2 shRNA KD as evidenced by decreased P-S6 intensity compared with untreated Tsc2 shRNA KD condition. Cells in rapamycin-treated Tsc2 shRNA-GFP animals exhibited P-S6 immunolabeling that was not different from that in scrambled shRNA controls. Quantification of P-S6 (S235/236) immunolabeling in scrambled shRNA-GFP, Tsc2 shRNA-GFP, and rapamycin-treated Tsc2 shRNA-GFP conditions represented as the mean intensity within the cell normalized to background intensity. *$P < 0.05$. $n = 5$ embryonic brains for scrambled and Tsc2 shRNA conditions, and $n = 4$ embryonic brains for Tsc2 + Rapamycin condition were analyzed. Scale bar: 10 μm. (*C*) Daily rapamycin treatment (5.0 mg/kg; E15-18) prevents increase in cell volume (cytomegaly) following Tsc2 shRNA KD. Confocal images of GFP-positive cells in (a) scrambled shRNA (region: UP_CP), (b) Tsc2 shRNA (region: IZ) and (c) rapamycin-treated Tsc2 shRNA (region: IZ) conditions. Scale bar: 14 μm. (d) Quantification of cell volume in scrambled shRNA (267.7 μm^3; $n = 7$), Tsc2 shRNA (408.4 μm^3; $n = 9$), and rapamycin-treated Tsc2 shRNA (162.8 μm^3; $n = 8$) conditions. *Scrambled shRNA versus Tsc2 shRNA, $P < 0.05$; #Tsc2 shRNA versus Tsc2 shRNA + Rapamycin, $P < 0.05$. (*D*) Rapamycin treatment prevented non-cell-autonomous effects following Tsc2 shRNA KD. Tsc2 shRNA KD results in a 2-fold increase in Cux1-positive cell in ROI surrounding GFP-positive cells ($n = 3$ embryonic brains) compared with scrambled shRNA control ($n = 4$ embryonic brains). Daily rapamycin treatment results in a significant decrease in the number of Cux1-positive cells surrounding the GFP-positive Tsc2 shRNA KD cells ($n = 3$ embryonic brains) compared with untreated Tsc2 shRNA condition. Quantification of Cux1-positive cells in ROI spanning IZ, LW_CP, MID_CP. *Scrambled shRNA versus Tsc2 shRNA, $P < 0.05$. #Tsc2 shRNA versus Tsc2 shRNA + rapamycin, $P < 0.05$. Scale bar: 100 μm.

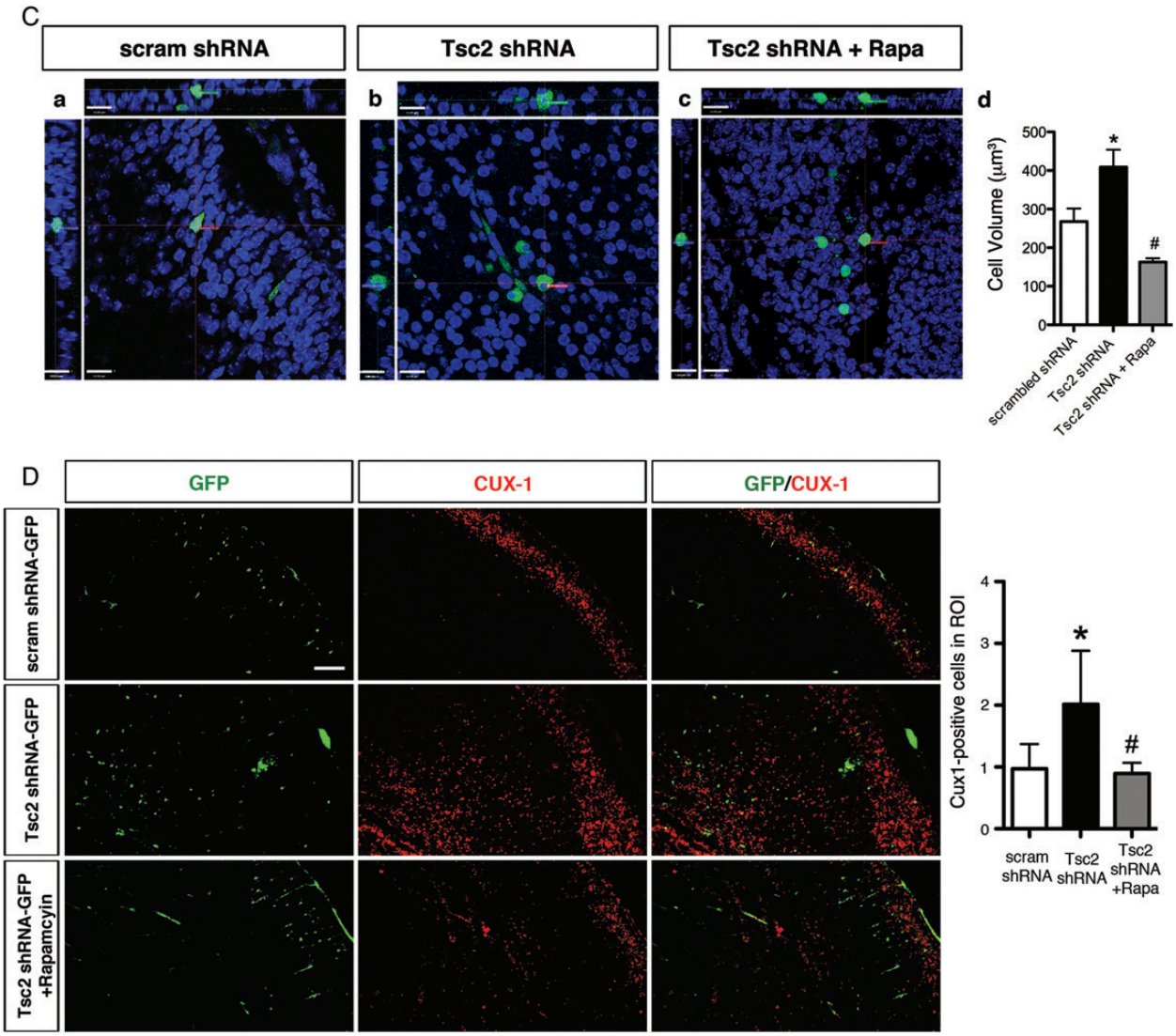

Figure 5. Continued

rapamycin (5.0 mg/kg) for 5 days (E14-E18). At E19, the percentage of BrdU-labeled cells reaching CP in rapamycin-treated animals (CP 75.3 ± 0.3%, IZ 10.3 ± 0.7%, VZ/SVZ 14.4 ± 0.5%; $n = 3$) did not significantly differ from untreated animals (CP 78.8 ± 2.0%, IZ 7.8 ± 0.7%, VZ/SVZ 13.4 ± 1.4%; $n = 4$; $P > 0.05$ for each region; Supplementary Fig. 5). However, incidental note was made of reduced brain weight and reduced body size following fetal rapamycin therapy (Supplementary Fig. 5).

Rapamycin Treatment Rescues Cytomegaly and Non-Cell-Autonomous Effects due to Tsc2 KD

Rapamycin treatment prevented cytomegaly (cell volume increase) in Tsc2 shRNA-transfected animals (162.8 µm^3 vs. untreated 408.4 µm^3; $P < 0.05$; Fig. 5*C*). Cell volume in rapamycin-treated Tsc2 shRNA animals was smaller than scrambled shRNA control cells (267.7 µm^3); however, it was not statistically significant ($P > 0.05$). Furthermore, treatment with rapamycin prevented the increase in the number of Cux1-positive cells surrounding GFP-positive cells in animals transfected with Tsc2 shRNA (Fig. 5*D*). Quantitative measurements were taken in the ROI surrounding the region of transfected GFP-positive cells and were quantified. Quantitative analysis revealed that the 2-fold increase in Cux1-positive cells in the ROI spanning IZ, LW_CP, and MID_CP regions was prevented with rapamycin treatment, and there was no significant difference between the number of Cux1-positive cells in ROI in rapamycin-treated Tsc2 shRNA animals compared with scrambled shRNA animals (Fig. 5*D*). These results suggest that mTORC1 inhibition during fetal development may prevent cell-autonomous effects as well as non-cell-autonomous effects of Tsc2 loss.

Discussion

We demonstrate for the first time the profile of mTORC1 and mTORC2 signaling cascade activation in human fetal tuber tissue. We provide data quantifying the significant cellular enlargement following Tsc2 KD in neural progenitor cells in vitro and in vivo and show that enhanced cell size can be prevented by rapamycin treatment. We demonstrate for the first

time that focal KD of Tsc2 during fetal brain development leads to a focal cortical lamination defect characterized by both cell-autonomous and non-cell-autonomous effects, that can be prevented by in utero rapamycin treatment. The effects of rapamycin on mTOR signaling have been studied in the postnatal rodent brain however little is known of the effects of rapamycin on mTOR signaling during fetal brain development, an epoch that coincides with the pathogenesis of TSC. Taken together, these data suggest that hyperactive mTORC1 and mTORC2 signaling in neural progenitor cells leads to cellular features of TSC, and that these effects could in theory be targeted therapeutically during in utero development.

Our findings support the hypothesis that mTORC1 activation is an early finding in fetal TSC brain lesions and provide a new window to understand the cellular pathogenesis of TSC. Of course, we acknowledge that only 4 specimens were analyzed, however, given the rarity of fetal TSC brain specimens, we were fortunate to assess 4 high-quality tissue samples. As alterations in cortical lamination that likely reflect nascent tubers have been reported in the fetal period by autopsy and magnetic resonance imaging studies (Park et al. 1997; Levine et al. 1999; Chen et al. 2010), we propose that mTORC1 hyperactivation is an early event in the pathogenesis of embryonic tuber formation (Crino 2010). The detection of P-p70S6K1, P-S6, and c-myc provides strong evidence that enhanced mTORC1 signaling in a focal region of the developing brain is intimately linked to abnormal architecture characteristic of tubers.

mTORC2 signaling, evidenced by increased levels of P-PKCα, P-Akt, P-SGK1, and P-NDRG1 is activated in the TSC adult and fetal brain specimens. Our findings differ from previous reports in human renal angiomyolipomas, $Tsc2^{+/-}$ mouse kidney angiomyolipomas, $Tsc2^{-/-}$ mouse embryonic fibroblasts, and human embryonic kidney 293 (HEK293) cells (Yang et al. 2006; Huang et al. 2008; Huang et al. 2009), which show that mTORC2 signaling cascade is attenuated in the absence of Tsc2. The disparity between these data and our own may reflect differential effects of mTORC2 in fetal neurons, or the presence of other modulators that are activated in TSC brain such as EGFR (Parker et al. 2011) that activate mTORC2 (Tanaka et al. 2011). In the adult tubers specimens, a possible contribution to changes in mTORC2 signaling from recurrent seizures is also possible. Two studies (Goto et al. 2011; Carson et al. 2012) have investigated mTORC2 substrates in brain lysates following *Tsc1* conditional knockout. In the *Emx-Tsc1* conditional knockout mouse strain (Carson et al. 2012), there was a reduction in phospho-NDRG1 at P15, whereas in the inducible in *Tsc1cc Nestin-rtTA + TetOp-cre* + strain (Goto et al. 2011), there was a reduction in P-PKCα at P30. Neither of these studies examined embryonic tissue or neural progenitor cells.

There have been few studies to date providing data quantifying the effects of Tsc2 KD or mTOR hyperactivation on cell size in neural progenitor cells although conditional knockout of *Tsc2* in radial glial cells in vivo causes enhanced cell size (Way et al. 2009). KD of Tsc2 in mNPCs resulted in a 2-fold increase in cell size associated with enhanced mTOR activation. The effect on cell size was preventable with rapamycin treatment suggesting that cytomegaly in TSC is an mTORC1-dependent process. Similar mechanistic effects on cell size have been demonstrated in the mouse for 2 other known mTORC1 inhibitory proteins, PTEN and STRADα (Kwon et al. 2003; Orlova, Parker et al. 2010), suggesting that mTORC1 signaling plays a pivotal role in cell size in the brain. Thus, mTORC1 inhibition may provide a potentially attractive strategy to prevent cytomegaly in neural progenitor cells. Further studies to define the precise role or mTORC2 activation in fetal TSC brain tissue are clearly warranted.

KD of Tsc2 during embryonic brain development resulted in a focal cortical lamination with the majority of cells being localized in deeper regions of the cortex instead of superficial layers II–III. This potentially suggests that Tsc2 plays a role in migration. It was interesting to find that only 21% of Tsc2 KD GFP-positive cells were Cux1-positive, while the other 79% were Cux1-negative. Homeobox Cux1 transcription factor has been shown to regulate dendrite branching, development of spines, and synapse formation of layer II/III neurons (Cubelos et al. 2010). Given that cells electroporated with Tsc2 shRNA do not migrate appropriately and in addition majority do not express Cux1 could potentially result in dysregulated neuronal development (e.g., spines and dendrite branching) and aberrant targeting and synapse formation. Furthermore, the Tsc2 KD cells that started on their migrational route but were localized in the IZ and lower CP regions (LW_CP, MID_CP), did not express transcription factors Ctip2 and Tbr1 that are specific to deeper cortical layers V and VI, indicating that at least at this stage in development, they have not taken on the cell identity of another cortical layer which surrounds them.

The observation that Tsc2 KD leads to altered laminar destination of Cux1-positive nontransfected cells suggests that there may be non-cell-autonomous effects of loss of Tsc2 function in the developing brain. It has previously been reported that RNAi KD of doublecortin gene *DCX* during brain development results in non-cell-autonomous defect in migration of neighboring cells (Bai et al. 2003). It is possible that Tsc2 KD results in mTORC1 hyperactivation, which in turn results in expression and secretion of factors that disrupt lamination of neighboring Cux1-positive cells. For example, following Tsc2 KD, mTORC1 activation could result in release of secretable factors that influence migration and lamination of surrounding progenitor cells. We have previously demonstrated robust expression of numerous growth factors including NT4, VEGF, HGF, and EGF in tubers and in the $Tsc1^{GFAP}Cre$ conditional mouse strain (Kyin et al. 2001; Parker et al. 2011) that could alter laminar destinations of migrating neurons.

While the existing conditional TSC mouse models provide invaluable systems to study brain development in TSC, rapamycin only partially reverses the structural abnormalities in these strains. In the $Tsc1^{syn}Cre$ mouse strain (Meikle et al. 2007), treatment with rapamycin or RAD001, another mTOR inhibitor, improves survival and reduces neuronal enlargement in vivo (Meikle et al. 2008), but disorganized neocortical architecture is not fully rescued possibly because rapamycin and RAD001 were begun at postnatal timepoints. Similarly, postnatal treatment with rapamycin in both $Tsc1^{GFAP}Cre$ (Zeng et al. 2008) and $Tsc2^{GFAP}Cre$ (Zeng et al. 2010) mice ameliorated the seizure phenotype but only partially rectified the histopathological abnormalities. Rapamycin has not been previously assayed as a preventative approach for Tsc2-induced lesions in utero, however, in a previous study, prenatal rapamycin improved survival of $Tsc1^{nestin}Cre$ conditional knockout mice (Anderl et al. 2011). Our results demonstrate

for the first time that the selective effects of Tsc2 KD on neural progenitor cells or during fetal brain development (e.g., cytomegaly, altered cortical lamination, and enhanced mTOR signaling) can be prevented with rapamycin treatment. In concert with the discovery of mTOR cascade hyperactivation in fetal tuber specimens, we suggest the possibility that prenatal treatment with mTOR pathway inhibitors could prevent or reduce neurological disability in TSC. In 2 recent clinical trials (Bissler et al. 2008; Krueger et al. 2010), tuber size was not altered following treatment with the rapamycin analog everolimus, and seizures were reduced in only 50% of patients (age range: 3–34 years) receiving the drug (Krueger et al. 2010). However, white matter abnormalities in TSC can be reversed with everolimus (Tillema et al. 2012). Postnatal treatment with mTOR inhibitors may miss a critical period in the pathogenesis of tuber formation and thus have limited benefit for all neurological features of TSC. However we acknowledge that rapamycin has independent effects on development including reduction of body size and brain weight, alterations in gene expression, and cognitive function (Ruegg et al. 2007; Way et al. 2012) that require important consideration for further clinical studies.

Supplementary Material

Supplementary material can be found at: http://www.cercor.oxfordjournals.org/

Funding

This work was supported by the National Institute of Neurological Disease and Stroke at the National Institutes of Health (NS045022 to P.B.C.), the PENN-Pfizer Collaborative Program; and Department of Defense CDMRP TSC Initiative (to P.B.C.); the National Epilepsy Fund—"Power of the Small," Hersenstichting Nederland (NEF 02-10 and NEF 05-11); and Stichting Michelle (M06.011; to E.A.).

Notes

We thank Dr Robert Fraser, who referred one fetal specimen to Dr Harvey Sarnat for neuropathological examination from the IWK Medical Centre, Halifax, Nova Scotia, Canada. We also thank Dr John Wolfe (Children's Hospital of Philadelphia, Philadelphia, PA) for the generous gift of mNPCs and his laboratory for help with the methods for isolating and culturing them; Dr Elizabeth Henske (Dana Farber Cancer Center, Boston, MA) for the generous gift of *Tsc2* null mouse embryonic fibroblasts; and Dr Dennis Kolson (University of Pennsylvania Perelman School of Medicine, Philadelphia, PA) for helpful discussion of this project and his laboratory for technical assistance. We also thank Stephanie Cross, Denise Cook, Tanya Weerakkody, Kevan Salimian, Jason Yoon, Jelte Helferrich, Julie Chen, and Alexander Gill for technical help and assistance with this project. *Conflict of Interest:* None declared.

References

Anderl S, Freeland M, Kwiatkowski DJ, Goto J. 2011. Therapeutic value of prenatal rapamycin treatment in a mouse brain model of tuberous sclerosis complex. Hum Mol Genet. 20:4597–4604.

Arlotta P, Molyneaux BJ, Chen J, Inoue J, Kominami R, Macklis JD. 2005. Neuronal subtype-specific genes that control corticospinal motor neuron development in vivo. Neuron. 45:207–221.

Bai J, Ramos RL, Ackman JB, Thomas AM, Lee RV, LoTurco JJ. 2003. RNAi reveals doublecortin is required for radial migration in rat neocortex. Nat Neurosci. 6:1277–1283.

Bissler JJ, McCormack FX, Young LR, Elwing JM, Chuck G, Leonard JM, Schmithorst VJ, Laor T, Brody AS, Bean J et al. 2008. Sirolimus for angiomyolipoma in tuberous sclerosis complex or lymphangioleiomyomatosis. N Engl J Med. 358:140–151.

Carson RP, Van Nielen DL, Winzenburger PA, Ess KC. 2012. Neuronal and glia abnormalities in Tsc1-deficient forebrain and partial rescue by rapamycin. Neurobiol Dis. 45:369–380.

Chen B, Schaevitz LR, McConnell SK. 2005. Fezl regulates the differentiation and axon targeting of layer 5 subcortical projection neurons in cerebral cortex. Proc Natl Acad Sci USA. 102:17184–17189.

Chen CP, Su YN, Chang TY, Liu YP, Tsai FJ, Chen MR, Hwang JK, Chen TH, Wang W. 2010. Prenatal diagnosis of rhabdomyomas and cerebral tuberous sclerosis by magnetic resonance imaging in one fetus of a dizygotic twin pregnancy associated with a frameshift mutation in the TSC2 gene. Taiwan J Obstet Gynecol. 49:387–389.

Crino PB. 2010. The pathophysiology of tuberous sclerosis complex. Epilepsia. 51(Suppl 1):27–29.

Crino PB, Nathanson KL, Henske EP. 2006. The tuberous sclerosis complex. N Engl J Med. 355:1345–1356.

Cubelos B, Sebastian-Serrano A, Beccari L, Calcagnotto ME, Cisneros E, Kim S, Dopazo A, Alvarez-Dolado M, Redondo JM, Bovolenta P et al. 2010. Cux1 and Cux2 regulate dendritic branching, spine morphology, and synapses of the upper layer neurons of the cortex. Neuron. 66:523–535.

DiMario FJ Jr. 2004. Brain abnormalities in tuberous sclerosis complex. J Child Neurol. 19:650–657.

Ess KC, Roach ES. 2012. New therapies for tuber-less sclerosis: white matter matters? Neurology. 78:520–521.

Feliciano DM, Su T, Lopez J, Platel JC, Bordey A. 2011. Single-cell Tsc1 knockout during corticogenesis generates tuber-like lesions and reduces seizure threshold in mice. J Clin Invest. 121:1596–1607.

Fingar DC, Salama S, Tsou C, Harlow E, Blenis J. 2002. Mammalian cell size is controlled by mTOR and its downstream targets S6K1 and 4EBP1/eIF4E. Genes Dev. 16:1472–1487.

Garcia-Martinez JM, Alessi DR. 2008. mTOR complex 2 (mTORC2) controls hydrophobic motif phosphorylation and activation of serum- and glucocorticoid-induced protein kinase 1 (SGK1). Biochem J. 416:375–385.

Goto J, Talos DM, Klein P, Qin W, Chekaluk YI, Anderl S, Malinowska IA, Di Nardo A, Bronson RT, Chan JA et al. 2011. Regulable neural progenitor-specific Tsc1 loss yields giant cells with organellar dysfunction in a model of tuberous sclerosis complex. Proc Natl Acad Sci USA. 108:E1070–1079.

Guertin DA, Sabatini DM. 2007. Defining the role of mTOR in cancer. Cancer Cell. 12:9–22.

Hevner RF, Shi L, Justice N, Hsueh Y, Sheng M, Smiga S, Bulfone A, Goffinet AM, Campagnoni AT, Rubenstein JL. 2001. Tbr1 regulates differentiation of the preplate and layer 6. Neuron. 29:353–366.

Huang J, Dibble CC, Matsuzaki M, Manning BD. 2008. The TSC1-TSC2 complex is required for proper activation of mTOR complex 2. Mol Cell Biol. 28:4104–4115.

Huang J, Manning BD. 2008. The TSC1-TSC2 complex: a molecular switchboard controlling cell growth. Biochem J. 412:179–190.

Huang J, Wu S, Wu CL, Manning BD. 2009. Signaling events downstream of mammalian target of rapamycin complex 2 are attenuated in cells and tumors deficient for the tuberous sclerosis complex tumor suppressors. Cancer Res. 69:6107–6114.

Jambaque I, Cusmai R, Curatolo P, Cortesi F, Perrot C, Dulac O. 1991. Neuropsychological aspects of tuberous sclerosis in relation to epilepsy and MRI findings. Dev Med Child Neurol. 33:698–705.

Krueger DA, Care MM, Holland K, Agricola K, Tudor C, Mangeshkar P, Wilson KA, Byars A, Sahmoud T, Franz DN. 2010. Everolimus for subependymal giant-cell astrocytomas in tuberous sclerosis. N Engl J Med. 363:1801–1811.

Kwon CH, Zhu X, Zhang J, Baker SJ. 2003. mTor is required for hypertrophy of Pten-deficient neuronal soma in vivo. Proc Natl Acad Sci USA. 100:12923–12928.

Kyin R, Hua Y, Baybis M, Scheithauer B, Kolson D, Uhlmann E, Gutmann D, Crino PB. 2001. Differential cellular expression of neurotrophins in cortical tubers of the tuberous sclerosis complex. Am J Pathol. 159:1541–1554.

Levine D, Barnes PD, Madsen JR, Abbott J, Mehta T, Edelman RR. 1999. Central nervous system abnormalities assessed with prenatal magnetic resonance imaging. Obstet Gynecol. 94:1011–1019.

Magnitsky S, Walton RM, Wolfe JH, Poptani H. 2008. Magnetic resonance imaging detects differences in migration between primary and immortalized neural stem cells. Acad Radiol. 15:1269–1281.

Marcotte L, Aronica E, Baybis M, Crino PB. 2012. Cytoarchitectural alterations are widespread in cerebral cortex in tuberous sclerosis complex. Acta Neuropathol. 123:685–693.

Marcotte L, Crino PB. 2006. The neurobiology of the tuberous sclerosis complex. Neuromol Med. 8:531–546.

Meikle L, Pollizzi K, Egnor A, Kramvis I, Lane H, Sahin M, Kwiatkowski DJ. 2008. Response of a neuronal model of tuberous sclerosis to mammalian target of rapamycin (mTOR) inhibitors: effects on mTORC1 and Akt signaling lead to improved survival and function. J Neurosci. 28:5422–5432.

Meikle L, Talos DM, Onda H, Pollizzi K, Rotenberg A, Sahin M, Jensen FE, Kwiatkowski DJ. 2007. A mouse model of tuberous sclerosis: neuronal loss of Tsc1 causes dysplastic and ectopic neurons, reduced myelination, seizure activity, and limited survival. J Neurosci. 27:5546–5558.

Molyneaux BJ, Arlotta P, Hirata T, Hibi M, Macklis JD. 2005. Fezl is required for the birth and specification of corticospinal motor neurons. Neuron. 47:817–831.

Nguyen L, Besson A, Heng JI, Schuurmans C, Teboul L, Parras C, Philpott A, Roberts JM, Guillemot F. 2006. p27kip1 independently promotes neuronal differentiation and migration in the cerebral cortex. Genes Dev. 20:1511–1524.

Nieto M, Monuki ES, Tang H, Imitola J, Haubst N, Khoury SJ, Cunningham J, Gotz M, Walsh CA. 2004. Expression of Cux-1 and Cux-2 in the subventricular zone and upper layers II-IV of the cerebral cortex. J Comp Neurol. 479:168–180.

Orlova KA, Parker WE, Heuer GG, Tsai V, Yoon J, Baybis M, Fenning RS, Strauss K, Crino PB. 2010. STRADalpha deficiency results in aberrant mTORC1 signaling during corticogenesis in humans and mice. J Clin Invest. 120:1591–1602.

Orlova KA, Tsai V, Baybis M, Heuer GG, Sisodiya S, Thom M, Strauss K, Aronica E, Storm PB, Crino PB. 2010. Early progenitor cell marker expression distinguishes type II from type I focal cortical dysplasias. J Neuropathol Exp Neurol. 69:850–863.

Park SH, Pepkowitz SH, Kerfoot C, De Rosa MJ, Poukens V, Wienecke R, DeClue JE, Vinters HV. 1997. Tuberous sclerosis in a 20-week gestation fetus: immunohistochemical study. Acta Neuropathol. 94:180–186.

Parker WE, Orlova KA, Heuer GG, Baybis M, Aronica E, Frost M, Wong M, Crino PB. 2011. Enhanced epidermal growth factor, hepatocyte growth factor, and vascular endothelial growth factor expression in tuberous sclerosis complex. Am J Pathol. 178:296–305.

Ruegg S, Baybis M, Juul H, Dichter M, Crino PB. 2007. Effects of rapamycin on gene expression, morphology, and electrophysiological properties of rat hippocampal neurons. Epilepsy Res. 77:85–92.

Saito T. 2006. In vivo electroporation in the embryonic mouse central nervous system. Nat Protoc. 1:1552–1558.

Samuel-Abraham S, Leonard JN. 2010. Staying on message: design principles for controlling nonspecific responses to siRNA. FEBS J. 277:4828–4836.

Sparagana SP, Roach ES. 2000. Tuberous sclerosis complex. Curr Opin Neurol. 13:115–119.

Tanaka K, Babic I, Nathanson D, Akhavan D, Guo D, Gini B, Dang J, Zhu S, Yang H, De Jesus J et al. 2011. Oncogenic EGFR signaling activates an mTORC2-NF-kappaB pathway that promotes chemotherapy resistance. Cancer Discov. 1:524–538.

Tillema JM, Leach JL, Krueger DA, Franz DN. 2012. Everolimus alters white matter diffusion in tuberous sclerosis complex. Neurology. 78:526–531.

Uhlmann EJ, Wong M, Baldwin RL, Bajenaru ML, Onda H, Kwiatkowski DJ, Yamada K, Gutmann DH. 2002. Astrocyte-specific TSC1 conditional knockout mice exhibit abnormal neuronal organization and seizures. Ann Neurol. 52:285–296.

Wang Y, Greenwood JS, Calcagnotto ME, Kirsch HE, Barbaro NM, Baraban SC. 2007. Neocortical hyperexcitability in a human case of tuberous sclerosis complex and mice lacking neuronal expression of TSC1. Ann Neurol. 61:139–152.

Way SW, McKenna J 3rd, Mietzsch U, Reith RM, Wu HC, Gambello MJ. 2009. Loss of Tsc2 in radial glia models the brain pathology of tuberous sclerosis complex in the mouse. Hum Mol Genet. 18:1252–1265.

Way SW, Rozas NS, Wu HC, McKenna J 3rd, Reith RM, Hashmi SS, Dash PK, Gambello MJ. 2012. The differential effects of prenatal and/or postnatal rapamycin on neurodevelopmental defects and cognition in a neuroglial mouse model of tuberous sclerosis complex. Hum Mol Genet. 21:3226–3236.

Wullschleger S, Loewith R, Hall MN. 2006. TOR signaling in growth and metabolism. Cell. 124:471–484.

Yang Q, Inoki K, Kim E, Guan KL. 2006. TSC1/TSC2 and Rheb have different effects on TORC1 and TORC2 activity. Proc Natl Acad Sci USA. 103:6811–6816.

Zaroff CM, Barr WB, Carlson C, LaJoie J, Madhavan D, Miles DK, Nass R, Devinsky O. 2006. Mental retardation and relation to seizure and tuber burden in tuberous sclerosis complex. Seizure. 15:558–562.

Zeng LH, McDaniel S, Rensing NR, Wong M. 2010. Regulation of cell death and epileptogenesis by the mammalian target of rapamycin (mTOR): a double-edged sword? Cell Cycle.. 9:2281–2285.

Zeng LH, Rensing NR, Zhang B, Gutmann DH, Gambello MJ, Wong M. 2011. Tsc2 gene inactivation causes a more severe epilepsy phenotype than Tsc1 inactivation in a mouse model of tuberous sclerosis complex. Hum Mol Genet. 20:445–454.

Zeng LH, Xu L, Gutmann DH, Wong M. 2008. Rapamycin prevents epilepsy in a mouse model of tuberous sclerosis complex. Ann Neurol. 63:444–453.